Available online at www.sciencedirect.com
SCIENCE DIRECT®
International Journal of Multiphase Flow 30 (2004) 225–236
International Journal of Multiphase Flow
www.elsevier.com/locate/ijmulflow

Brief communication

Two-phase flow pattern maps for vertical upward gas–liquid flow in mini-gap channels

Pongsiri Satitchaicharoen, Somchai Wongwises *

Fluid Mechanics, Thermal Engineering and Multiphase Flow Research Lab (FUTURE), Department of Mechanical Engineering, King Mongkut's University of Technology Thonburi, 91 Prachautit Road, Bangmod, Bangkok 10140, Thailand

Received 21 July 2003; received in revised form 25 November 2003

1. Introduction

Gas–liquid two-phase flow through a confined gap is encountered in several engineering applications including the cooling systems of various types of equipment such as high performance micro-electronics, supercomputers, high-powered lasers, medical devices, high heat-flux compact heat exchangers in spacecraft and satellites etc. It can be expected that the restriction of the bubble space in the minichannel is the cause of the difference in the two-phase flow characteristics from those in conventional channel geometries. This may also affect heat-mass transfer characteristics during the change of phase.

It is not possible to understand the two-phase flow phenomena without a clear understanding of the flow patterns encountered. It is expected that the flow patterns will influence the two-phase pressure drop, holdup, system stability, exchange rates of momentum, heat and mass during the phase-change heat transfer processes. The ability to predict the type of flow accurately is necessary before the relevant calculation techniques can be developed.

Two-phase flow patterns in small circular tubes have been studied by a number of researchers. In contrast, the flow patterns of upward gas–liquid two-phase flow in mini non-circular channels have received comparatively little attention in literature.

In order to elucidate the effect of inertia and surface tension in microchannels at microgravity, Zhao and Rezkallah (1993) proposed the phasic Weber number as system parameters. Their flow regime map was divided into three zones; surface tension-dominated zone (bubbly and slug flow regimes), inertia-dominated zone (annular flow regime) and the transition zone.

Wilmarth and Ishii (1994, 1997) observed the flow patterns, and measured the void fraction and the interfacial area concentration of adiabatic co-current vertical and horizontal air–water flow in

* Corresponding author. Tel.: +662-470-9115; fax: +662-470-9111.
E-mail address: somchai.won@kmutt.ac.th (S. Wongwises).

0301-9322/$ - see front matter
doi:10.1016/j.ijmultiphaseflow.2003.11.006

narrow rectangular channels with gaps of 1 and 2 mm. The developed flow regime maps were compared with that obtained for a round pipe.

Bonjour and Lallemand (1998) performed experiments to elucidate the flow regimes of natural convective boiling of R113 in upward two-phase flow in vertical narrow rectangular channels with the gap sizes ranging between 0.5 and 2 mm. Three flow boiling regimes, namely nucleate boiling with isolated deformed bubbles, nucleate boiling with coalesced bubbles, and partial dry out, were observed. A new flow regime map based on the Bond number and a ratio of the heat flux to the critical heat flux was developed to confine the boiling.

Xu (1999a,b) investigated an adiabatic co-current vertical two-phase flow of air and water in vertical rectangular channels (12 mm $\times$ 260 mm) with narrow gaps of 0.3, 0.6 and 1.0 mm. Flow patterns for gaps of 0.6 and 1.0 mm were similar to those reported in the literature. By decreasing the channel gaps, the transition from one flow regime to another appeared at a lower gas velocity. However, for the gaps of 0.3 mm, even at very low gas flow rate, bubbly flow was never found.

Hibiki and Mishima (2001) developed a mathematical model to predict the flow regime transition for vertical upward flows in narrow rectangular channels. The model was based on that of Mishima and Ishii (1984) for vertical upward two-phase flows in round tubes. The developed model was compared with the measured data of air–water flows in rectangular channels with gaps of 0.3–17 mm.

Zhao and Bi (2001) conducted experiments to visualize the co-current upward air–water two-phase flow patterns in vertical equilateral triangular channels with hydraulic diameters of 0.866, 1.443 and 2.886 mm. The observed flow patterns obtained from the larger hydraulic diameters (1.443 and 2.886 mm) were found to be similar to those obtained from conventional, large-sized vertical circular tubes. For the smallest channel (0.866 mm), the dispersed bubbly flow pattern was not found.

Akbar et al. (2003) compared the measured data reported in open literature with a Weber number-based two-phase flow regime map which was previously developed by Zhao and Rezkallah (1993), and Rezkallah (1996). Balasubramanian and Kandlikar (2003) used the high speed photography for observation of flow behaviors (nucleate boiling, slug formation, dryout, reverse flow and flow at the exit manifold) during flow boiling of water in a single rectangular minichannel.

As mentioned above, relatively little information is currently available on experimental work on flow patterns in narrow rectangular channels, and in particular detailed investigations are lacking on the effects of gap size, channel width and liquid viscosity on the flow patterns and flow pattern maps. In the present study, the main objective is to obtain and clarify the characteristics of flow patterns in vertical upward co-current gas–liquid two-phase flow in mini-gap rectangular channels. The effects of gap size, channel width, and liquid viscosity on the flow patterns and flow pattern maps, which have never before appeared in open literature, are presented.

2. Experimental apparatus and procedure

The main components of the system consisted of a vertical test section, an air supply, and a water supply. Air–water, air-20 wt.% glycerol solution, and air-40 wt.% glycerol solution were used as working fluids. The densities of air, water, 20 wt.% glycerol solution and 40 wt.% glycerol solution are 1.17, 10^3, 1.043×10^3 and 1.094×10^3 kg/m^3, respectively. The dynamic viscosities of

air, water, 20 wt.% glycerol solution and 40 wt.% glycerol solution are 1.86×10^{-5}, 8×10^{-4}, 11.6×10^{-4} and 22.8×10^{-4} Pa·s, respectively.

Five differently sized rectangular test sections as shown in Table 1 were made of transparent acrylic glass to permit visual observation of the flow patterns. The connections of the piping system were designed such that parts could be changed very easily. Liquid was pumped from the storage tank through the rotameter, the air–liquid mixture (Fig. 1) and the test section. Air was injected from a compressor to pass through the reservoir, the regulation valve, the flow meter, the mixer and the test section. Both the air and liquid streams were brought together in a mixer and then passed through the test section co-currently. The inlet flow rates of air and liquid were

Table 1
Sizes of the test section

No.	Channel width, W (mm)	Gap width, H (mm)	Channel length, L (mm)	Hydraulic diameter, D_h (mm)
1	40	1	1000	1.95
2	40	2	1000	3.81
3	40	3	1000	5.58
4	20	2	1000	3.63
5	60	2	1000	3.87

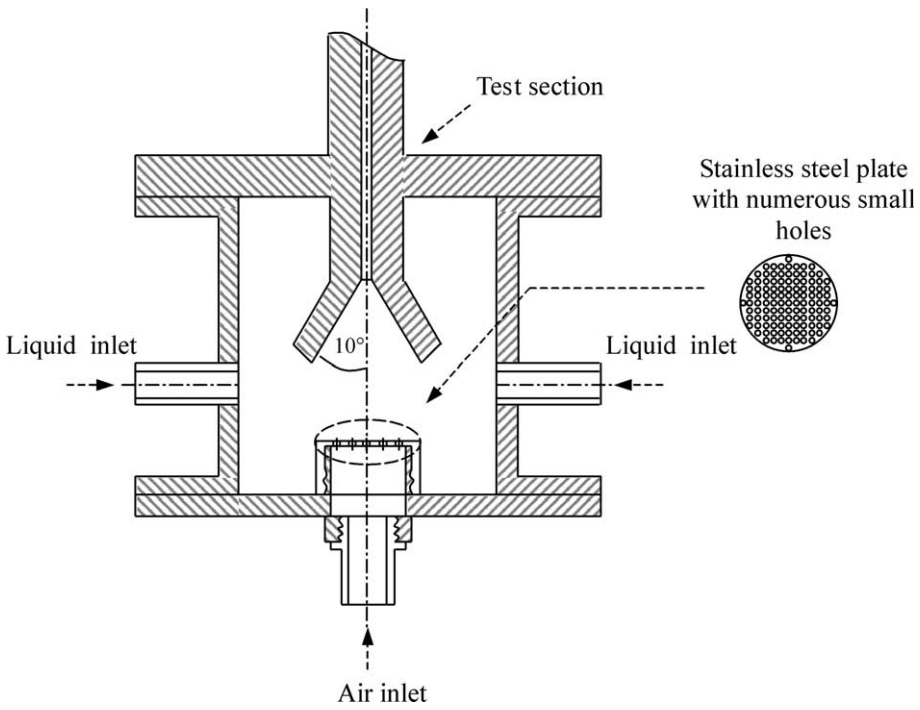

Fig. 1. Schematic diagram of air–liquid inlet section.

measured by means of several sets of rotameters. The flow meters for the glycerol solution were calibrated by the usual method.

It should be noted that the air–liquid entrance section was our latest development. It was designed and employed after problems were encountered from several entrance sections used in previous experiments. The air–liquid entrance section served to introduce liquid smoothly along the test section. The liquid from the air–liquid mixer flowed upward together with air, and then flowed back to the storage tank.

Experiments were conducted at various air and liquid flow rates to determine the flow regime maps. The air flow rate was increased by small increments while the liquid flow rate was kept constant at a pre-selected value. The process of each flow pattern formation was registered in detail by visual observation, video recorder, and digital camera (NIKON 385E). The system was allowed to approach steady conditions before the air and liquid flow rates were recorded.

3. Results and discussion

Visual observation shows that different flow patterns may occur with gas–liquid co-current upward flow in vertical mini-gap channels. Typical photographs of the flow patterns, in accordance with the results obtained between 0.2 and 0.7 m from the inlet of the test section, are shown in Figs. 2–6. The following flow patterns were obtained by increasing the air flow rate by small increments while the water flow rate was kept constant at pre-selected value. The different transfer

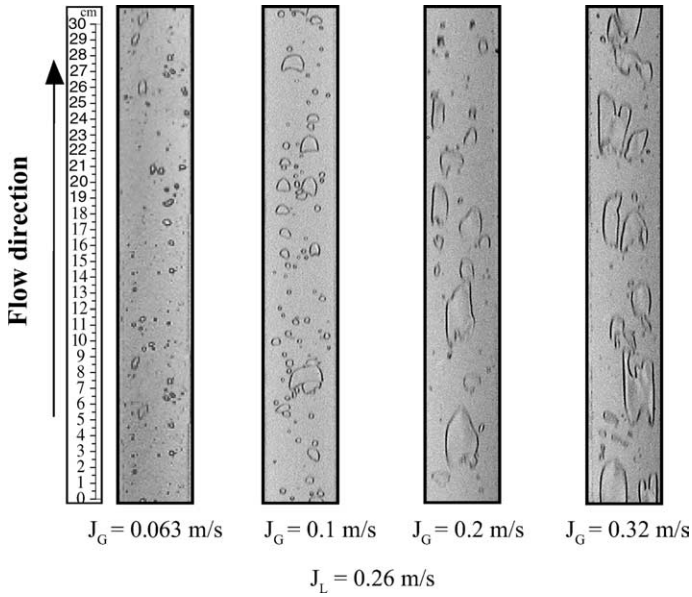

Fig. 2. Bubbly flow patterns (B) of air–water in a vertical channel with $H = 3$ mm and $W = 40$ mm.

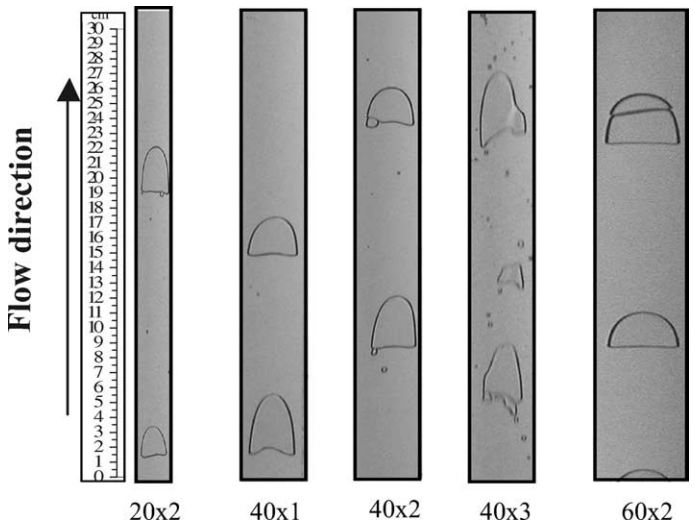

Fig. 3. Cap-bubbly flow patterns (CB) of air-40 wt.% glycerol solution in various test sections.

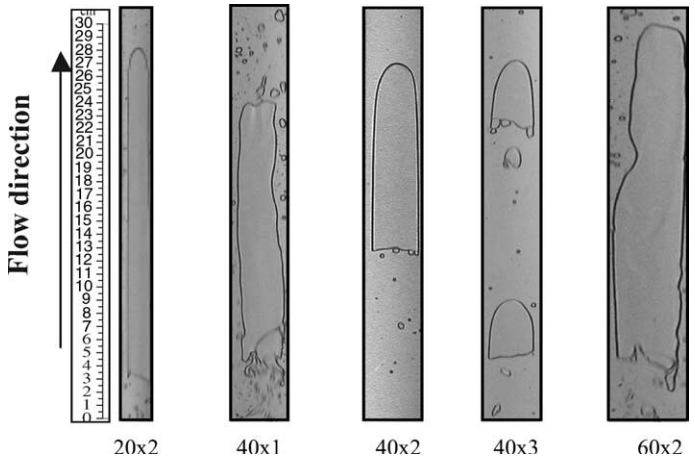

Fig. 4. Slug flow patterns (S) of air-40 wt.% glycerol solution in various test sections.

processes can be characterised from these figures. Descriptions of each flow pattern are defined as follows:

3.1. Bubbly flow (B)

The flowing liquid phase is continuous and contains a dispersion of small circular shaped bubbles of various sizes. Larger bubbles which are of an irregular shape, occur through combination of smaller ones. Fig. 2 shows the bubbly flow pattern at the 40×3 test section at various superficial air and water velocities (J_G and J_L).

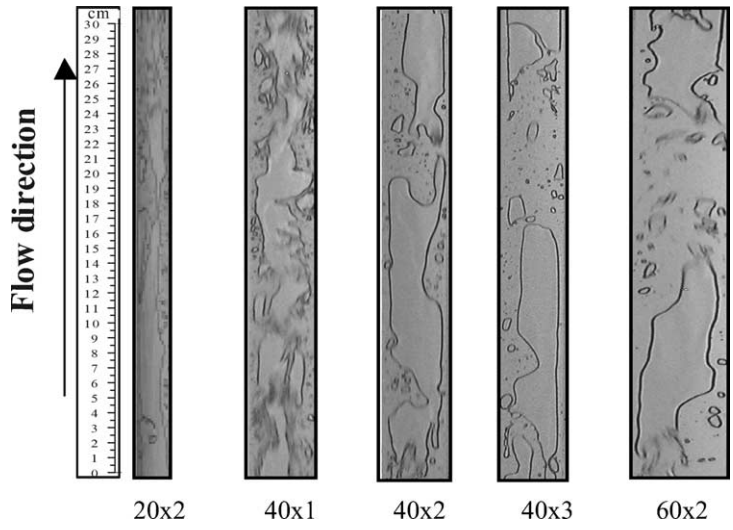

Fig. 5. Churn flow patterns (C) of air-40 wt.% glycerol solution in various test sections.

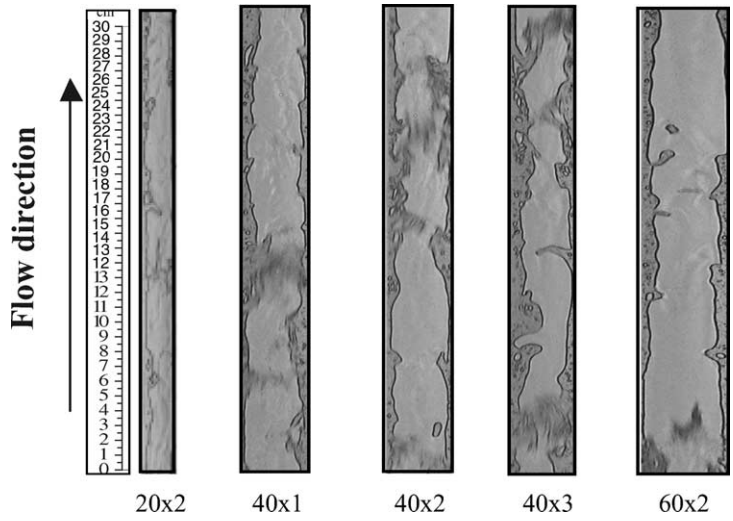

Fig. 6. Annular flow patterns (A) of air-40 wt.% glycerol solution in various test sections.

3.2. Cap-bubbly flow (CB)

With increasing air flow rate, many small bubbles are combined to form "half circular-shaped" bubbles. The diameter of these bubbles is almost equal to the channel width. The length of these bubbles is less than the channel width. The train of bubbles follows the channel line in the continuous liquid phase which may contain a dispersion of smaller bubbles. Fig. 3 shows the cap-bubbly flow pattern at various test sections tested with air-40 wt.% glycerol solution at $J_L = 0.26$ m/s and $J_G = 0.1$ m/s.

3.3. Slug flow (S)

Although similar to cap-bubbly flow, "bullet-shaped" bubbles are formed. These bubbles are longer and separated by liquid bridges containing a dispersion of smaller bubbles. Fig. 4 shows the slug flow pattern at various test sections tested with air-40 wt.% glycerol solution at $J_L = 0.26$ m/s and $J_G = 0.55$ m/s.

3.4. Churn flow (C)

Churn flow is formed by a breakdown of the slug flow bubbles. This leads to an oscillatory motion of the liquid downward and upward in the channel. Fig. 5 shows the churn flow pattern at various test sections tested with air-40 wt.% glycerol solution at $J_L = 0.26$ m/s and $J_G = 3.93$ m/s.

3.5. Annular flow (A)

This flow pattern is characterized by the complete separation of the liquid and gas phases, with flowing of the liquid film on the channel wall and gas in the channel core. The entire circumference of the channel wall is continuously wetted by a liquid film of non-uniform thickness. The gas–liquid interface is wavy due to the disturbance by the gas stream. Some of the small droplets may be entrained in the gas core. Fig. 6 shows the annular flow pattern at various test sections tested with air-40 wt.% glycerol solution at $J_L = 0.26$ m/s and $J_G = 8.85$ m/s.

It should be noted that the bubbly flow pattern was found only in the 40 mm × 3 mm rectangular channel for air–water. The usual method in the presentation of flow pattern data, is to classify the flow pattern by visual observation and plot the data as a flow pattern map in terms of system parameters e.g. superficial velocity, Weber number etc. Parameters used in the present study are the phase superficial velocities. The superficial velocity of gas (J_G) and of liquid (J_L) refer to the situation where the designated phase flows alone in the pipe. In the present study, both superficial velocities refer to average ambient conditions (1.013 bar, 30 °C). Fig. 7 shows two-phase flow data and flow pattern map for air-40 wt.% glycerol solution for $W = 40$ mm, $H = 1$ mm and $L = 1000$ mm. The solid lines in this figure represent the boundary of the flow patterns and transition from one flow pattern to another. Actually, due to the uncertainty at the vicinity of the transitions between flow patterns, the flow patterns do not change suddenly. Therefore, the transition lines should be represented as broad transition bands. The flow pattern map is valid in the range of 0.03–10 m/s for J_G, and 0.025–2 m/s for J_L. The flow pattern maps obtained from the present study are presented in Figs. 8–12.

Fig. 8 shows the flow pattern maps for air–water at a specific gap size of 2 mm for different widths of 20, 40 and 60 mm. Cap-bubbly flow, slug flow, churn flow and annular flow were observed from the experiments. The figure shows that at a specific gap size and a specific superficial liquid velocity and when the channel width is increased, the transition from the cap-bubbly flow region to the slug flow region (CB–S) shifts to a higher value of superficial air velocity. Identical shifts are seen for the slug flow region to the churn flow region (S–C) and the churn flow region to the flow region (C–A). Finally, the cap-bubbly flow region becomes larger, while the annular flow region becomes smaller. The reason for this is that when the channel width

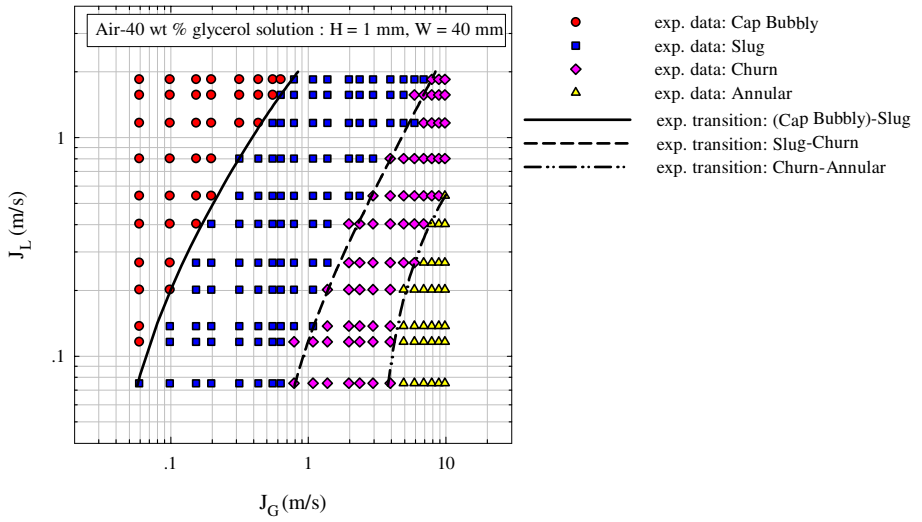

Fig. 7. Air-40 wt.% glycerol solution flow pattern map for the 1 mm gap and 40 mm channel width test section.

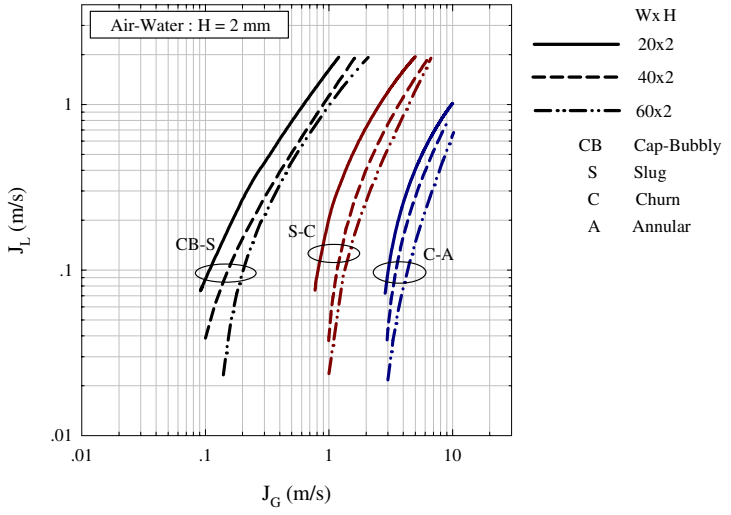

Fig. 8. Effect of channel width on the air–water flow pattern map for the 2 mm gap channel.

is larger, the bubbles are dispersed. The combining of smaller bubbles to become bigger ones remains more difficult as long as the air flow is not increased.

Effect of the gap size on the flow transition is shown in Fig. 9. As the channel width is fixed and the gap size is varied at a specific superficial liquid velocity, it is clear that the transition of each boundary line (CB–S, S–C, C–A) also shifts to a higher value of superficial air velocity. The cause of the boundary shift can be given in a similar way as in the previous case. As the channel gap increases, bubbles tend to be dependent. Therefore, one way of maintaining the flow condition is by increasing the air velocity. Comparison of the present flow pattern transitions for the 1 mm gap and

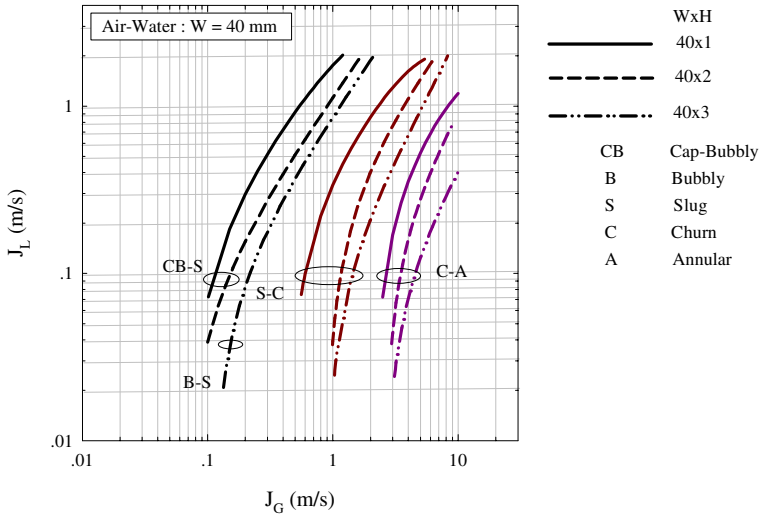

Fig. 9. Effect of gap width on the air–water flow pattern map for a vertical channel with $W = 40$ mm.

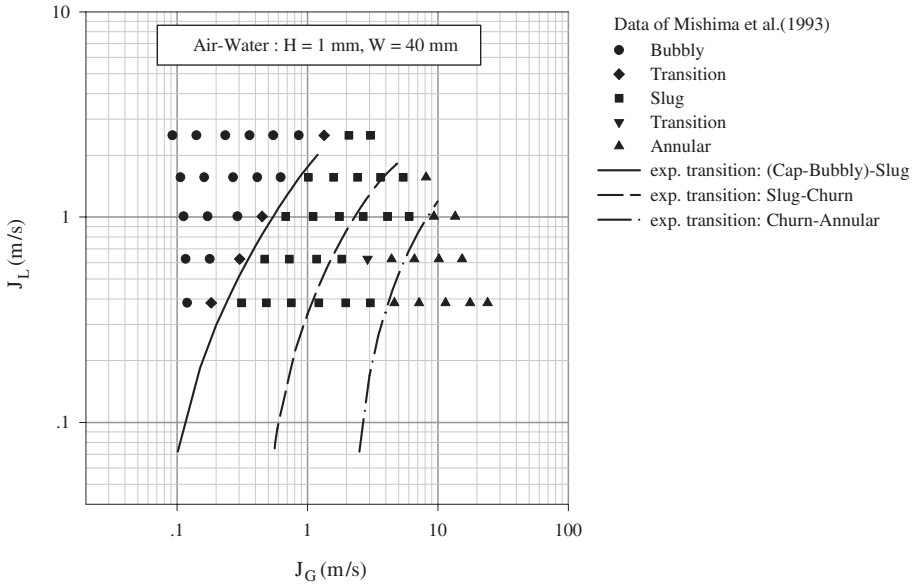

Fig. 10. Present flow pattern map compared with the experimental data of Mishima et al. (1993).

40 mm channel width test section with the experimental data of Mishima et al. (1993) is shown in Fig. 10. The transition line between the cap-bubbly flow (CB) and the slug flow (S) are in very good agreement with that between bubbly and slug flows data of Mishima et al. The regions of slug flow and annular flow obtained from the present study are also in very good agreement with those obtained from Mishima et al. The transition data between slug and annular flows of Mishima et al. is in the region of churn flow in the present study. The discrepancies from comparisons depend

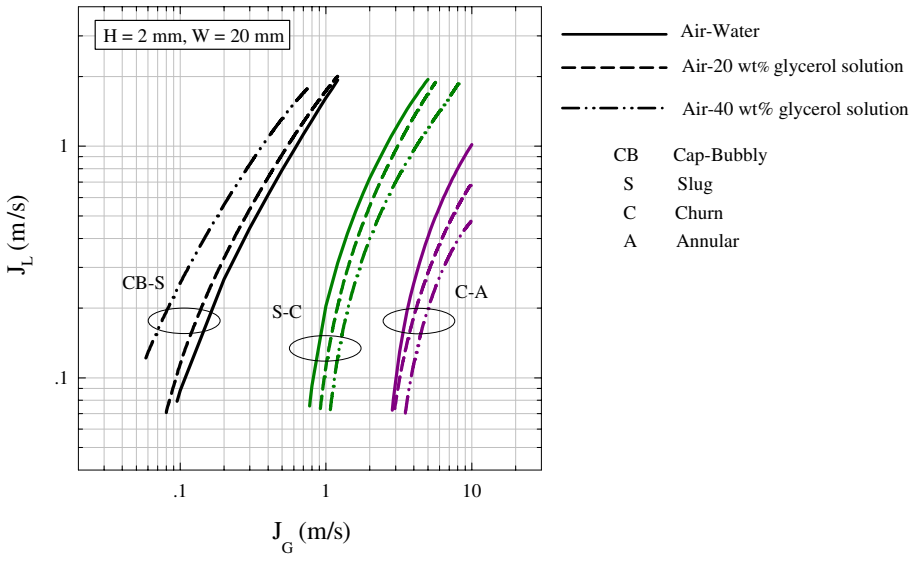

Fig. 11. Effect of viscosity on the flow pattern map for a vertical channel with $H = 2$ mm and $W = 20$ mm.

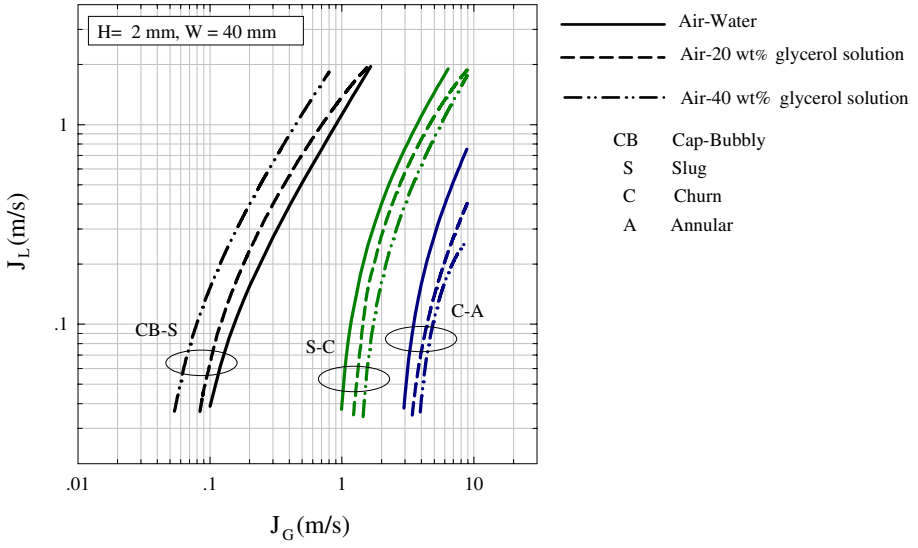

Fig. 12. Effect of viscosity on the flow pattern map for a vertical channel with $H = 2$ mm and $W = 40$ mm.

mainly on the identification of flow pattern according to their definitions and also the configurations of inlet and outlet sections. However, in general the results agree qualitatively.

Effects of liquid viscosity on the flow transition are shown in Figs. 11–13. It can be noted that the viscosity of 20 wt.% glycerol solution and 40 wt.% glycerol solution are 1.45 and 2.85 times as much as water, respectively. The effect of the viscosity on the transition lines between the cap-bubbly (CB) and the slug flow (S) is very interesting. At the same superficial liquid velocity, as

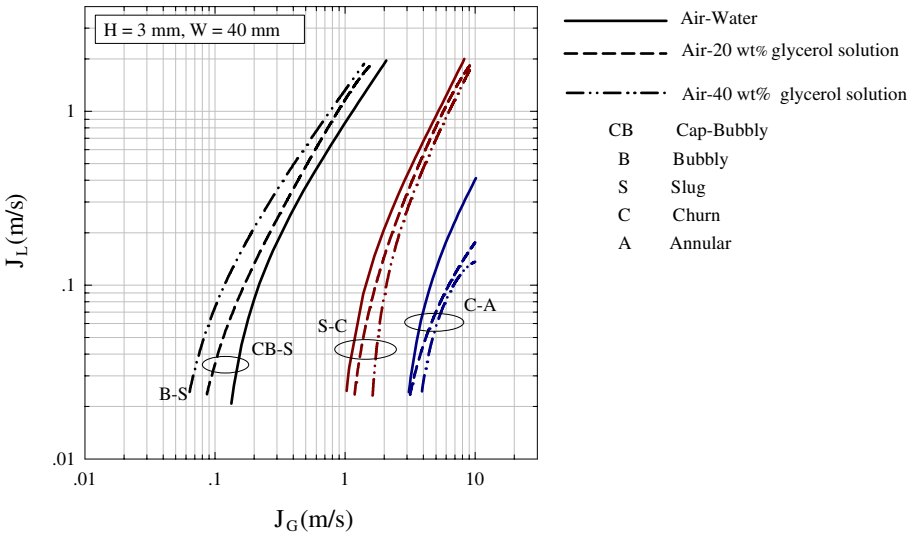

Fig. 13. Effect of viscosity on the flow pattern map for a vertical channel with $H = 3$ mm and $W = 40$ mm.

liquid with a higher viscosity was used, the CB–S transition line shifts to a lower value of superficial air velocity. This is different from the S–C transition line and the C–A transition line, which shift to a higher value of superficial air velocity at the same superficial liquid velocity. In fact, at the region of higher air velocity, as the viscosity of the liquid is higher, the higher shear stress resists the combination of the bubbles. The increase of the air velocity enables the flow pattern to be maintained. Therefore, using liquid with a higher viscosity results in the S–C and C–A transition lines moving to a higher value of superficial air velocity. In contrast, at the region of lower air velocity, the shear stress is also small. Liquid with a higher viscosity (lower surface tension) enables the bubbles to combine and become bigger ones more easily. This results in the shift of the CB-S transition line to the left.

4. Conclusion

This paper presents new data to clarify the flow patterns of vertical upward gas–liquid two-phase flow in mini-gap rectangular channels. Air–water, air-20 wt.% glycerol solution, and air-40 wt.% glycerol solution were used as working fluids. Various rectangular test sections: 20 mm × 2 mm, 40 mm × 1 mm, 40 mm × 2 mm, 40 mm × 3 mm and 60 mm × 2 mm at an equal length of 1 m, were used in the experiments. The air flow was slowly increased while the liquid flow was fixed at a pre-selected value. The flow phenomena, which were bubbly flow, cap-bubbly flow, slug flow, churn flow and annular flow, were observed and recorded by high-speed camera. Bubbly flow pattern was found only in the 40 mm × 3 mm rectangular channel for air–water. The flow pattern maps were presented as a function of the superficial velocity of both phases. The effects of gap size, channel width and liquid viscosity on the flow pattern transitions were examined. At a specific gap size, when the channel width is increased, the onset of transition from the cap-bubbly

flow region to the slug flow region (CB–S) shifted to a higher value of superficial air velocity. Identical shifts were found for the slug flow region to the churn flow region (S–C) and the churn flow region to the slug flow region (C–A). The same results were observed when the channel width was fixed and gap size was varied. The effect of viscosity on the flow pattern map is very interesting. For the same test section, as liquid with a higher viscosity was used, the CB–S transition line shifted to a lower value of superficial air velocity while the S–C transition line and the C–A transition line shifted to a higher value of superficial air velocity. The present flow pattern maps are based on the superficial velocities of air, water and glycerol solution all the transitions between two flow patterns are dependent on the fluid nature. Therefore, these maps may be not applicable to other fluids. However, the experimental results will be useful to provide a better understanding of the boiling behavior in mini channels. For further investigations, the phasic Weber numbers are recommended for the system parameters of the flow pattern transitions.

Acknowledgements

The present study was financially supported by the Thailand Research Fund (TRF) whose guidance and assistance are gratefully acknowledged.

References

Akbar, M.K., Plummer, D.A., Ghiaasiaan, S.M., 2003. On gas–liquid two-phase flow regimes in microchannels. Int. J. Multiphase Flow 29, 855–865.

Balasubramanian, P., Kandlikar, S.G., 2003. High speed photographic observation of flow patterns during flow boiling in single rectangular minichannel. In: ASME Summer Heat Transfer Conference, July 21–23, Las Vegas, Nevada, USA.

Bonjour, J., Lallemand, M., 1998. Flow patterns during boiling in a narrow space between two vertical surfaces. Int. J. Multiphase Flow 24, 947–960.

Hibiki, T., Mishima, K., 2001. Flow regime transition criteria for upward two-phase flow in vertical narrow rectangular channels. Nuclear Engineering and Design 203, 117–131.

Mishima, K., Ishii, M., 1984. Flow regime transition criteria for upward two-phase flow in vertical tubes. Int. J. Heat and Mass Transfer 27, 723–737.

Mishima, K., Hibiki, T., Nishihara, H., 1993. Some characteristics of gas–liquid flow in narrow rectangular ducts. Int. J. Multiphase Flow 19, 115–124.

Rezkallah, K.S., 1996. Weber number based flow pattern maps for liquid-gas flows at microgravity. Int. J. Multiphase Flow 22, 1265–1270.

Wilmarth, T., Ishii, M., 1994. Two-phase flow regime in narrow rectangular vertical and horizontal channels. Int. J. Heat and Mass Transfer 37, 1749–1758.

Wilmarth, T., Ishii, M., 1997. Interfacial area concentration and void fraction of two-phase flow in narrow rectangular vertical channels. J. Fluid Engineering 19, 916–922.

Xu, J., 1999a. Experimental study on gas–liquid two-phase flow regimes in rectangular channels with mini gaps. Int. J. Heat and Fluid Flow 20, 422–428.

Xu, J., Cheng, P., Zhao, T.S., 1999b. Gas–liquid two-phase flow regimes in rectangular channels with mini/micro gaps. Int. J. Multiphase Flow 25, 411–432.

Zhao, T.S., Bi, Q.C., 2001. Co-current air–water two-phase flow patterns in vertical triangular micro-channels. Int. J. Multiphase Flow 27, 765–782.

Zhao, L., Rezkallah, K.S., 1993. Gas–liquid flow patterns at microgravity condition. Int. J. Multiphase Flow 19, 751–763.